Non-reflecting boundary conditions for acoustic transfer matrix estimation with LES

By Wolfgang Polifke † AND Cliff Wall

The estimation of (thermo-)acoustic transfer matrices from numerically-generated time series of pressure and velocity fluctuations with correlation analysis appears to be an efficient and flexible way of employing CFD for the study of combustion instabilities. In the present investigation, the use of large-eddy simulation (LES) for this technique is explored for the first time. For this purpose, a novel formulation for boundary conditions, which is fully non-reflecting for plane acoustic waves, was derived, implemented and successfully tested. It was observed that large-scale turbulent fluctuations, which are explicitly resolved in LES, can generate spurious signal contributions inside the computational domain and additional acoustic waves at the outlet boundary of the domain. To allow accurate transfer matrix estimation with LES, these signal components must be suppressed or eliminated from the time-series data by suitable post-processing.

1. Introduction

Thermoacoustic instabilities are a cause for concern in combustion applications ranging from small household burners to rocket engines. The "brute-force" application of computational fluid mechanics (CFD) to the analysis of thermo-acoustic systems can be forbiddingly expensive due to the high computational demands of a time- and space-accurate simulation of a (low Mach number) compressible, turbulent, reacting flow. An efficient and often adequate description of the (thermo-)acoustic properties of a combustion system is provided by acoustic multi-port or "network" representations, see e.g. Bohn & Deuker (1993); Poinsot & Veynante (2001); Polifke *et al.* (2001*a*). Within this framework, both the response to an external or fluid-mechanic internal excitation as well as stability with respect to self-excited oscillations can be analyzed.

In order to represent a combustion system with these tools, the so-called *transfer matrices* of all multi-ports of the system must be known. The transfer matrices provide a mathematical description of the dynamical characteristics of a multi-port (within the limits of a linear analysis). For simple components, the transfer matrix can be derived from the (linearized) equations of conservation of mass and momentum and suitable additional assumptions. In general, however, the determination of the transfer matrix from first principles is not possible, and one has to resort to experiment (see e.g. Paschereit & Polifke (1998)) or numerical simulation.

Bohn and co-workers have suggested (see e.g. Bohn & Deuker (1993); Deuker (1995); Krüger *et al.* (1998)) determining the acoustic properties of an element - e.g. a burner or a flame - by numerically simulating and evaluating its response to a sudden disturbance. Specifically, the frequency response function $F(\omega)$ of a flame is obtained as the Laplace transform of the response (in the time domain) to a unit-step perturbation of the mass flux approaching the flame. It is thereby possible to determine the frequency

† Lehrstuhl für Thermodynamik, Technische Universität München, Germany

response function for a range of frequencies from one single time-dependent CFD simulation! Polifke *et al.* (1998, 2001*b*) have extended this idea, using modern tools of *system identification* (Ljung (1999); Bellanger (1984)) to determine the complete transfer *matrix* of an acoustic multi-port with time-lagged heat release and pressure loss ("n-τ-ζ model").

This advanced approach, known as *correlation analysis*, has since been applied by Gentemann *et al.* (2003) to turbulent pipe flow through a sudden change in cross section (an "area change") and successfully validated with experimental data. In that work, a RANS turbulence model was used. In the present paper – using the same simple geometry – the use of large eddy simulation for transfer matrix estimation with correlation analysis (TME) is explored for the first time. Emphasis is placed on the optimal choice of boundary conditions for successful transfer matrix estimation.

2. Correlation analysis basics

Consider the values of fluctuating variables up- and downstream of an acoustic element as *signals* s and *responses* r. A time-dependent numerical simulation will produce a time series $s_i = s(i\Delta t), i = 0, \ldots, N$ and similarly r_i. The coupling between signal and response is approximated as

$$r_i \approx \hat{r}_i = \sum_{k=0}^{L} h_k s_{i-k} \text{ for } i = L, \ldots, N. \tag{2.1}$$

In the terminology of digital signal processing or system identification, see e.g. Rabiner & Gold (1975); Bellanger (1984), (2.1) describes a *finite impulse response* (FIR) filter with *impulse response* $\underline{h}$.

The so-called *Wiener-Hopf equation* relates the *autocorrelation matrix* Γ of the signal $\underline{s}$ and the impulse-response vector $\underline{h}$ to the *cross-correlation* $\underline{c}$ between $\underline{s}$ and $\underline{r}$ (Ljung (1999); Bellanger (1984)):

$$\Gamma \underline{h} = \underline{c}, \tag{2.2}$$

For time-series data generated by time-dependent CFD, the auto- and cross-correlations are approximated as follows:

$$c_i \approx \frac{1}{N-L+1} \sum_{l=L}^{N} s_{l-i} r_l \text{ for } i = 0, \ldots, L, \tag{2.3}$$

$$\Gamma_{ij} \approx \frac{1}{N-L+1} \sum_{l=L}^{N} s_{l-i} s_{l-j} \text{ for } i, j = 0, \ldots, L. \tag{2.4}$$

The impulse response $\underline{h}$ is determined from time-series data by inversion of the Wiener-Hopf equation, (2.2). A frequency response $F(\omega)$ is then computed as the z-transform $H(z)$ of $\underline{h}$ with argument $z = \exp\{i\omega\Delta t\}$:

$$F(\omega) = H\left(e^{i\omega\Delta t}\right) = \sum_{k=0}^{L} h_k e^{-i\omega\Delta t k}. \tag{2.5}$$

3. Correlation analysis and acoustic multi-ports

The discussion in the previous section was limited to a scalar frequency response $F(\omega)$. However, an $m \times m$ transfer matrix describing an m-port filter can be estimated with correlation analysis if a signal vector $\underline{s}$, defined as a suitable combination of the m

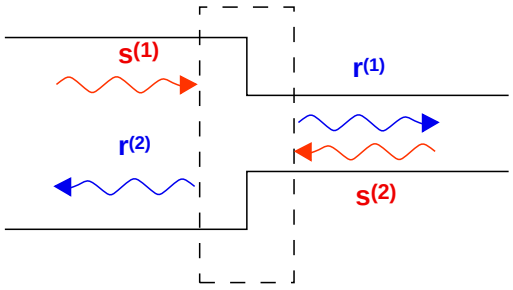

FIGURE 1. Incident acoustic waves as signals $s^{(1)}, s^{(2)}$ and reflected / transmitted waves as responses $r^{(1)}, r^{(2)}$ of an acoustic two-port.

signal variables $s^{(n)}, n = 1, \ldots, m$, and m impulse response functions $\underline{h}^{(n)}$ – one for each response port of the element - are introduced (Polifke *et al.* (2001*b*)). For acoustic systems, $m = 2$ typically and the variables s, r are the fluctuations of pressure $\tilde{p}$ and velocity $\tilde{u}$ or the in- and outgoing Riemann invariants f and g at the up- and downstream side of the acoustic multi-port, respectively (see figure 1 and section 4.2).

Estimation of a complete transfer matrix or scattering matrix from a single computation provides a significant advantage over alternative approaches (Deuker (1995), Poinsot & Veynante (2001)). Also note that the signal shape is quite arbitrary; superposed sine waves and in particular bandwidth-limited "white noise" have produced good results, while step functions – which are not easily represented accurately in a time-dependent fluid dynamics computation – can be avoided. The amount of data required to produce dependable estimates of auto- and crosscorrelation is not excessive. It is not required that initial transients die out completely, and simulation times of the order of just one period of the lowest frequencies involved have been found to be sufficient.

It is, however, required that the signals $s^{(n)}$ incident on the acoustic element be 1) broad-band, with fairly uniform amplitude throughout the frequency range of interest, to probe the system dynamics with adequate signal-to-noise ratio and 2) not degenerate, i.e. input signals $s^{(n)}$ at different ports must not be strongly correlated with each other. Otherwise, the Wiener-Hopf equation (2.2) is ill-conditioned and its inversion is very sensitive to numerical or statistical errors.

4. Boundary conditions

When estimating the acoustic transfer matrix with time-dpeendent CFD, the acoustic element of interest is usually only part of the computational domain; see figure 2. It follows from the discussion of required signal properties in the preceding section that particular attention must be paid to the definition of the boundary conditions. Wave processes at the boundary are shown in figure 2. Outgoing, reflected and external waves are expressed in terms of the Riemann invariants $f = f(x-(u+c)t)$ and $g = g(x-(u-c)t)$, traveling in the positive and negative x-direction, respectively.

The Riemann invariants are related to fluctuations (denoted by "˜") of acoustic pressure and velocity as follows:

$$\frac{\tilde{p}}{\rho c} = f + g, \quad \tilde{u} = f - g, \tag{4.1}$$

$$f = \frac{1}{2}\left(\frac{\tilde{p}}{\rho c} + \tilde{u}\right), \quad g = \frac{1}{2}\left(\frac{\tilde{p}}{\rho c} - \tilde{u}\right). \tag{4.2}$$

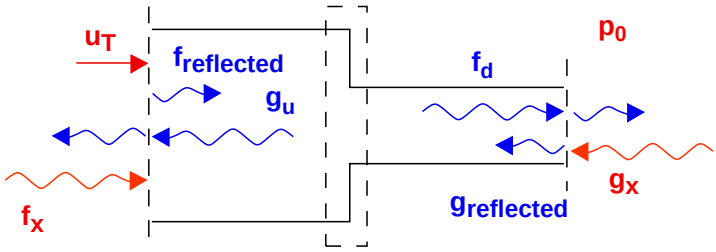

FIGURE 2. Boundaries of computational domain with outgoing waves g_u, f_d and forcing f_x, g_x at inlet and outlet, respectively. Reflected and transmitted wave components are also shown. The dashed line indicates the acoustic multi-port, i.e. the area change.

For harmonic waves with angular frequency ω,

$$f(x,t) = \hat{f}e^{i(\omega t - k_{x+}x)},\ g(x,t) = \hat{g}e^{i(\omega t - k_{x-}x)}. \tag{4.3}$$

Here $k_{x\pm} \equiv \pm\omega/c(1 \pm M)$ are the wave numbers of the invariants, and the "$\hat{}$" indicates a complex-valued wave amplitude.

As indicated in figure 2, the boundary conditions must first provide an excitation signal of suitable amplitude and frequency content. However, in general the signals $s^{(1)}$ and $s^{(2)}$ are related neither directly nor uniquely to external waves f_x and g_x imposed at the boundary. If there is reflection of outgoing waves at the boundary, then the signal $s^{(1)}$, say, will be influenced strongly by $f_{\text{reflected}}$, and similarly for the outlet. A closed feedback loop of acoustic waves traveling in the up- and downstream directions throughout the system is established, resulting in significant correlation between signals $s^{(1)}$ and $s^{(2)}$. Resonant amplification near acoustic eigenmodes of the acoustic system will lead to large signal amplitudes at the eigenfrequencies, which will dominate the autocorrelation matrix in an undesirable manner. These effects will make robust estimation of the transfer matrix difficult or impossible. It follows that the boundary conditions must be formulated in such a way that outgoing acoustic waves are not reflected back into the computational domain.

Finally, the boundary conditions must maintain certain values for the target velocity u_T – which in the case of large-eddy simulation includes a time-dependent turbulent component – at the inlet, as well as the far-field pressure p_∞ at the outlet.

4.1. *Characteristics-based boundary conditions*

A strategy for defining boundary conditions in compressible viscous flow is outlined in Thompson (1987) and Poinsot & Lele (1992). The boundary conditions are formulated in terms of characteristic wave relations. In the present context, acoustic waves with incidence normal to a boundary are of particular interest. If the boundary lies in the (y,z)-plane, say, the corresponding boundary conditions are formulated with the help of two quantities $\mathcal{L}_5$ and $\mathcal{L}_1$ defined as follows:

$$\mathcal{L}_i \equiv \lambda_i \left(\frac{\partial p}{\partial x} \pm \rho c \frac{\partial u}{\partial x} \right), \tag{4.4}$$

where the "+" sign corresponds to the index "5", and the $\lambda_i \equiv u \pm c$ are propagation speed of the waves. It has been shown by Poinsot & Lele (1992), that the $\mathcal{L}_i$'s can be interpreted as the time variations of wave amplitudes at the boundary.

4.2. *LODI relations and Riemann invariants*

Poinsot & Lele (1992) introduced local one-dimensional inviscid (LODI) relations to obtain approximate values for the wave-amplitude variations in terms of the primitive flow variables. For pressure and the velocity component normal to the boundary, the expressions

$$\frac{\partial p}{\partial t} + \frac{1}{2}\left(\mathcal{L}_5 + \mathcal{L}_1\right) = 0, \qquad \frac{\partial u}{\partial t} + \frac{1}{2\rho c}\left(\mathcal{L}_5 - \mathcal{L}_1\right) = 0 \tag{4.5}$$

are given. In the present context, plane harmonic waves are of particular interest, so – using the definitions (4.4) and (4.2) – we express the wave-amplitude variations $\mathcal{L}$ and the LODI relations in terms of the Riemann invariants. Subtracting the second part of (4.5) from the first, one obtains

$$\frac{\partial}{\partial t}\left(\frac{\tilde{p}}{\rho c} - \tilde{u}\right) + \frac{1}{\rho c}\mathcal{L}_1 = 0 \;\text{ or }\; \mathcal{L}_1 = -i\,2\omega\rho c\; g, \tag{4.6}$$

with (4.2) and $\partial g/\partial t = i\omega g$ for harmonic waves. Similarly,

$$\mathcal{L}_5 = -i\,2\omega\rho c\; f. \tag{4.7}$$

4.3. *(Partially) reflecting boundary conditions*

In this section, various types of boundary conditions, which can be implemented with the approach proposed in Poinsot & Lele (1992), are presented and their acoustic properties are briefly discussed.

4.3.1. *Subsonic reflecting outlet – "open end"*

A subsonic reflecting outlet should correspond to an "open-end" boundary condition in acoustics, where $\tilde{p} = f + g = 0$. Indeed we infer from (4.6) and (4.7) that $\mathcal{L}_1 + \mathcal{L}_5 = 0$ at an "open end", which is equivalent to equation (38) in Poinsot & Lele (1992). Note that an open-end boundary is strongly reflecting, with a reflection factor $r = -1$. (The reflection factor r is defined as the ratio of the reflected to the outgoing Riemann invariant, e.g. $r = g/f$ at an outlet, provided that there is no external incoming acoustic signal.)

4.3.2. *Subsonic partially-reflecting outlet*

If the temporal evolution of velocity and pressure at an outlet ($x = L$) would be determined solely from an outgoing wave $\mathcal{L}_5$ via the appropriate LODI relation, then – neglecting viscous and multidimensional effects – the outgoing wave would leave the domain without reflection.

However, the static pressure at the boundary must be "informed" somehow about the plenum or far-field pressure p_∞. Poinsot & Lele (1992) suggest prescribing, for this purpose, an ingoing wave at a flow outlet as

$$\mathcal{L}_1 = \frac{\sigma c}{L}(p - p_\infty), \tag{4.8}$$

where σ is a coupling parameter which is to be chosen appropriately. The speed of sound c and length L are introduced for dimensional consistency and represent characteristic scales of the problem. Then, if there is no outgoing wave $\mathcal{L}_5$, we see with (4.5) that an excess pressure $\Delta p = p - p_\infty$ will be reduced exponentially to zero according to

$$\frac{\partial \Delta p}{\partial t} = -\frac{\sigma c}{2\,L}\Delta p, \tag{4.9}$$

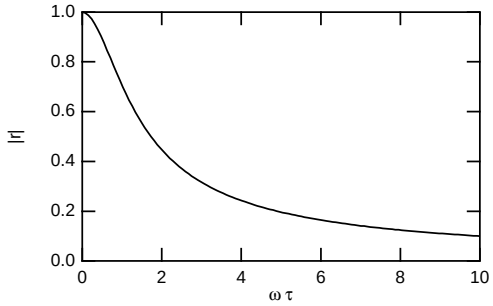

FIGURE 3. Absolute value of reflection coefficient $|r|$ vs. non-dimensional frequency $\omega\tau$ for partially reflecting in- or outflow boundary condition according to (4.8) and (4.13).

with a decay time

$$\tau \equiv \frac{2\,L}{\sigma c} \tag{4.10}$$

inversely proportional to the coupling coefficient σ.

Unfortunately, with such a prescription the boundary is no longer truly non-reflecting, because the pressure p which appears in (4.8) depends both on the in- as well as the outgoing waves. The reflection coefficient $r = g/f$ for plane waves at an outflow boundary, which is set up according to (4.8), can be estimated as follows: Assuming that pressure deviations from the prescribed value p_∞ at the outlet are dominated by acoustic waves f, g with angular frequency ω, (4.6) yields

$$r = \frac{g}{f} = \frac{\sigma c/L\,(p - p_\infty)}{-2i\,\rho c\,\omega\,f} \approx \frac{i\,\sigma c}{2\omega L}\frac{f+g}{f} = \frac{i}{\omega\tau}(1+r). \tag{4.11}$$

Solving for r, a complex-valued reflection coefficient is obtained:

$$r = \frac{-1}{1+i\omega\tau} = \begin{cases} i\,0 & \text{for } \omega\tau \to \infty \text{ (high-frequency limit),} \\ -1 & \text{for } \omega\tau \to 0 \text{ (low-frequency limit).} \end{cases} \tag{4.12}$$

For waves with relatively high frequency – with a period of oscillation much smaller than the decay constant τ – the restoration of the pressure at the outlet according to (4.8) is too slow to respond to the acoustic perturbations, such that the boundary is indeed effectively non-reflecting. Conversely, a low-frequency signal is reflected as if it had encountered an "open end" ($\tilde{p} = 0$), because the boundary condition (4.8) succeeds in keeping the pressure at the outlet close to the target value p_∞ due to the comparatively short decay time constant τ.

4.3.3. *Subsonic partially-reflecting inlet*

In order to have correct turbulence statistics at an inlet, the flow velocity u has to be imposed, which leads to difficulties in the definition of a fully-non-reflecting boundary condition very similar to those described in the previous subsection. From the LODI relations (4.5), one infers that with

$$\mathcal{L}_5 = \frac{\sigma c}{L}\rho c(u - u_T) \tag{4.13}$$

a deviation of the inflow velocity from the target value u_T should again decay exponentially with a time constant $2L/\sigma c$. For the reflection coefficient one obtains

$$r = \frac{f}{g} = \frac{1}{1 + i\omega\tau} = \begin{cases} -i\,0 & \text{for } \omega\tau \to \infty \text{ (high-frequency limit)}, \\ 1 & \text{for } \omega\tau \to 0 \text{ (low-frequency limit)}. \end{cases} \tag{4.14}$$

i.e. in the low-frequency limit the boundary condition (4.13) acts like a "closed end" without (acoustic) fluctuations of velocity.

In figure 3, the absolute value of the reflection coefficient $|r|$ is plotted as a function of the non-dimensional frequency $\omega\tau$. The absolute value $|r|$ of the reflection coefficient is the same for (4.12) and (4.14). If the magnitude of the reflection coefficient $|r|$ is not to exceed a certain value for a given frequency ω, then the corresponding minimum time constant τ can be deduced from this plot. Unfortunately, large values of τ correspond to low values of the coupling coefficient σ, which may result in divergence of the flow solver or drift of the values of velocity and pressure from the target values u_T and p_∞, respectively.

To summarize, although the boundary conditions (4.8) and (4.13) are often referred to as "non-reflecting" boundary conditions in the literature, they will lead to significant reflection of outgoing waves for sufficiently low frequencies. In thermo-acoustic problems unstable modes often correspond to low-order eigenmodes ("1/4-wave"-mode, etc.), and the corresponding low frequencies are of particular interest.

Note that Selle (2002) has independently obtained similar results concerning the frequency-dependence of the reflection coefficient by integrating a differential equation for pressure perturbations resulting from Eqns. (4.8) and (4.13).

4.3.4. *Boundaries with incoming waves*

With the help of (4.6) and (4.7), wave amplitudes $\tilde{\mathcal{L}}_1$ and $\tilde{\mathcal{L}}_5$ corresponding to external waves f_x and g_x can be specified as additional terms in the boundary conditions,

$$\mathcal{L}_i = \ldots + \tilde{\mathcal{L}}_i, \tag{4.15}$$

where "..." stands for the coupling terms discussed above, or terms which correspond to inflow turbulence.

For example, if a random number generator and a Butterworth filter are used to generate a time series $f_x(t)$ with uniform power spectral density over a certain range of frequencies, then the time derivative of this series provides the related wave amplitude variation $\tilde{\mathcal{L}}_5$,

$$\tilde{\mathcal{L}}_5 = -2\rho c \frac{\partial f_x(t)}{\partial t}, \tag{4.16}$$

see Eqn. (4.6). If the incoming signal is a superposition of sine-waves, then the corresponding wave amplitude variation equals

$$\tilde{\mathcal{L}}_5 = -2\rho c \sum A_n \omega_n \cos(\omega_n t + \phi_n). \tag{4.17}$$

4.4. *Plane wave non-reflecting boundary conditions*

It is possible to construct boundary conditions which – at least for plane waves with normal incidence – should be nearly non-reflecting even at low frequencies $\omega\tau \to 0$. The idea is to identify plane waves impinging on the boundary either from the outside (e.g. an excitation signal f_x or g_x) or from the inside, and then eliminate the plane wave contribution to the velocity coupling term (4.13) at an inflow boundary, and similarly for the pressure coupling (4.8) at an outflow. The use of an absorbing "sponge layer"

is often not possible in thermo-acoustic problems due to the very low frequencies and correspondingly large wave lengths typically involved. In the case of an inflow, these considerations suggest:

$$\mathcal{L}_5 = \frac{\sigma c}{L}\rho c\,(u - (f_x - g) - u_T) + \tilde{\mathcal{L}}_5. \tag{4.18}$$

Similarly, for an outflow,

$$\mathcal{L}_1 = \frac{\sigma c}{L}\,(p - \rho c\,(f + g_x) - p_\infty) + \tilde{\mathcal{L}}_1. \tag{4.19}$$

4.4.1. *Area-averaged reflection coefficient for plane waves*

In order to determine the reflection coefficient resulting from (4.18) or (4.19) for outgoing plane waves, we recall that plane waves which are incident normally to a boundary exhibit – with the exception of the acoustic boundary layer, which is usually very thin – no spatial variation over the boundary. Therefore, as far as plane waves are concerned, the reflection coefficient for an inflow boundary, say, may be written as follows:

$$r = \langle\frac{\mathcal{L}_5}{\mathcal{L}_1}\rangle \approx \frac{\langle\mathcal{L}_5\rangle}{\langle\mathcal{L}_1\rangle}\left(1 - \frac{\langle\mathcal{L}_5'\mathcal{L}_1'\rangle}{\langle\mathcal{L}_5\rangle\langle\mathcal{L}_1\rangle}\right) \approx \frac{\langle\mathcal{L}_5\rangle}{\langle\mathcal{L}_1\rangle} = \frac{i\sigma c}{2\omega L}\left(\frac{\langle u - u_T\rangle - (f - g)}{g}\right). \tag{4.20}$$

Here an (instantaneous) area average over the inflow boundary and local deviations from this average are denoted as $\langle\ldots\rangle$ and "$\ldots'$", respectively. For the application that we have in mind, it is reasonable to assume that the incoming and outgoing $\mathcal{L}$s are not strongly correlated, $\langle\mathcal{L}_5'\mathcal{L}_1'\rangle \approx 0$, while $\langle f\rangle = f$ and similarly for the outgoing Riemann invariant g. The boundary condition (4.18) has been employed, and of course the external forcing $\mathcal{L}_5$ is not considered in the determination of the reflection coefficient.

It follows that the reflection coefficient r indeed vanishes for plane harmonic waves of arbitrary frequency if one can assume that the area-averaged deviations of velocity from the target value are primarily due to plane acoustic waves at the boundary, because in this case $\langle u - u_T\rangle = f - g$.

Similar arguments suggest that an outflow boundary condition satisfying (4.19) should also be non-reflecting even at very low frequencies. Again, it must be assumed that area-averaged deviations of pressure from the target value p_∞ are primarily due to the plane acoustic waves – whether this assumption actually holds true in LES computations will be discussed below.

4.4.2. *Estimation of Riemann invariants at the boundary*

The Riemann invariants in (4.18) and (4.19) must be determined from the boundary conditions or the primitive variables at grid points at or near the boundary. By design, the area-averaged amplitude variation of the incoming waves f_x, g_x should be well approximated by the external excitation signal,

$$\langle\mathcal{L}_5\rangle \approx \tilde{\mathcal{L}}_5, \tag{4.21}$$

and it is has been shown in section 4.3.4 how the external Riemann invariants are related to the wave amplitude variations $\mathcal{L}_1$ and $\mathcal{L}_5$.

The outgoing waves must be constructed from interior grid points. At an inlet, say, we assume that area-averaged deviations δu and δp from the target values u_T and p_0 (the steady state average pressure at the inlet) are due to harmonic waves only, i.e.

$$g(t) = \frac{1}{2}\left(\frac{\delta p}{\rho c} - \delta u\right), \tag{4.22}$$

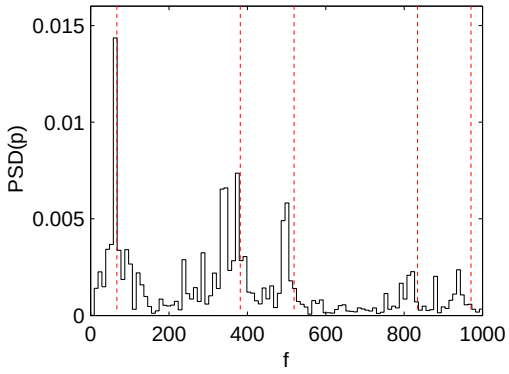

FIGURE 4. Power spectral distribution of pressure at the area change in LES simulation. The dotted lines indicate acoustic eigenfrequencies with "closed end" and "open end" boundary conditions up- and downstream, respectively.

where $\delta u \equiv \langle u - u_T \rangle$, $\delta p \equiv \langle p - p_0 \rangle$, and similarly for an outflow boundary.

5. Simulation results

An LES of the configuration shown in figure 2, with an area ratio of 4:1 and a total length of 0.8 m, has been performed using the method of Wall *et al.* (2002). This method is an extension of the low Mach number method of Pierce (2001) to compressible flow, and is efficient at low Mach number without introducing any artificial damping of acoustic waves. Turbulent inflow data for u_T as well as the v and w components of velocity at the inlet plane are obtained from a separate, incompressible, channel flow calculation using the method of Pierce (2001). Both quasi-two- and three-dimensional simulations have been performed, using a mean velocity of 7 m/s at the inlet, and a time step of 1.5×10^{-5} s. At each time step the code generates averaged values of both pressure and streamwise velocity at planes $0.5, 0.10, 0.20, 0.30$, and 0.38 m from the plane of the contraction in both the up- and downstream directions.

A simulation with the partially-reflecting boundary conditions according to (4.8) and (4.13) and broadband excitation both up- and downstream produced the power spectral distribution of pressure at the area change shown in figure 4. Strong resonance peaks are observed, suggesting that the boundaries are strongly reflecting (non-reflecting boundaries would yield a uniform PSD). Indeed, the location of the strongest peaks agrees reasonably well with the acoustic eigenfrequencies (indicated by the dotted lines in the figure) predicted by a simple acoustic network-model of this configuration with "closed end" and "open end" boundary conditions up- and downstream, respectively.

These observations prompted the investigation of the acoustic properties of partially reflecting boundary conditions described in Sections 4.3.2, 4.3.3 and the new formulation for boundary conditions described in Section 4.4. Reflection factors actually observed with the new and old formulations for the inflow boundary are shown in figure 5. In this run, the maximum possible time constant is $\tau = 8.4 \times 10^{-5}$ s. With larger values of τ, i.e. a smaller coupling constants σ for the inflow velocity, the solver diverges. According to Eqn. (4.13) this value should yield, even for the highest frequency $f = 1000$ Hz considered, a reflection factor close to unity. This is confirmed by LES results obtained with the old formulation for the inflow boundary (4.14), while the new formulation results in a very

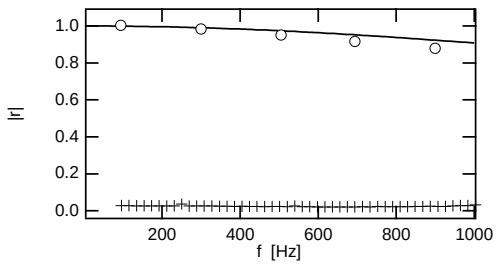

FIGURE 5. Inlet reflection factors observed in LES computations with boundary conditions (4.13) (∘) and (4.18) (+), respectively and according to Eqn. (4.14) (——).

small reflection factor even at the lowest frequencies $f = 100$ Hz considered in these runs; see figure 5. Note that the coherence – expressed as a normalized, oversampled cross-power spectral density – between signals $s^{(1)}$ and $s^{(2)}$ is significantly influenced by the boundary conditions: the coherence is very close to unity when the reflection factor is large, while it fluctuates between 0 and 1 with a mean value of approximately 0.4 with the new boundary conditions (not shown).

At the outflow, near-zero reflection factors cannot be observed, no matter which boundary condition is used. When using the standard formulation (4.8) at the outlet, it is possible to work with a rather low value of the coupling coefficient σ, corresponding to a time constant $\tau = 0.02$ s, without divergence or "drift" of the outlet pressure. Thus one should – according to (4.12) or figure 3 – expect a near-zero reflection coefficient $|r| < 0.01$ for $f = 1000$, while for frequencies around 100 Hz $|r| \approx 0.08$. Instead, reflection coefficients larger than unity are observed, i.e. the upstream-traveling Riemann invariant g is larger than its companion f traveling in the downstream direction – even for frequency bands where there is no forcing signal g_x imposed at the outlet. Similar results are obtained with the new formulation (4.19) for the outflow boundary.

The explanation proposed for these findings is that turbulent fluctuations originating from the contraction 1) generate spurious signals ("pseudo-sound") at the monitor planes downstream of the contraction 2) give rise to upstream-travelling acoustic waves g as they impinge on the downstream boundary. This hypothesis is supported by power spectrum distributions of the signals $s^{(1)}$ (the downstream-traveling wave f on the upstream side of the contraction) and $s^{(2)}$ (the upstream wave g downstream of the contraction) observed in an LES run, where both the upstream and downstream forcing functions, f_x and g_x, comprise a sum over 20 sinusoids of equal amplitude in the frequency range 50 – 1000 Hz. The PSD of $s^{(1)}$ shows as expected 20 equally spaced peaks of approximately equal amplitude, while the spectrum of $s^{(2)}$ displays amplitudes which vary significantly and are overall much larger than expected, see figure 6. Also, the location of the peaks does not correspond well to the spectrum of g_x.

These spurious contributions to the signals recorded at the monitor planes make it impossible to reconstruct the transfer matrix of the area change with acceptable accuracy from the LES data (not shown). Conversely, in unsteady RANS calculations, turbulent fluctuations are not explicitly resolved, and the agreement between computed and measured transfer matrices is very good and agrees well with theoretical expectations as well as experimental results, see Gentemann *et al.* (2003)

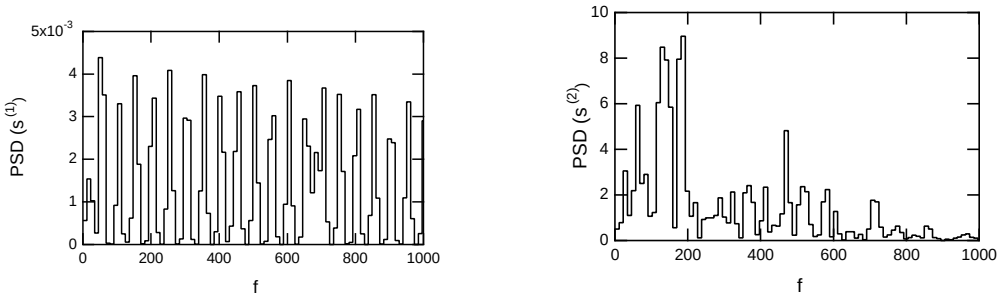

FIGURE 6. Power spectral distributions of signals $s^{(1)}$ (left) and $s^{(2)}$ (right) with plane-wave non-reflecting boundary conditions and broad-band sinusoidal external forcing at inflow and outflow boundaries

6. Conclusion

The estimation of (thermo-)acoustic transfer matrices from numerically-generated time series of pressure and velocity fluctuations through correlation analysis is arguably a flexible and efficient way of employing CFD for the study of combustion instabilities. First investigations based on unsteady laminar flow and Reynolds-averaged Navier-Stokes formulations for turbulent flow have shown promising results. In this study, the utilization of large eddy simulation for this technique is explored for the first time.

To this purpose, a novel formulation for boundary conditions was derived, implemented and successfully tested: it allows plane acoustic waves to leave the computational domain without reflection – even at very low frequencies, where the standard formulation for partially reflecting boundaries is strongly reflecting.

However, it was not possible to reconstruct the transfer matrix of the simple test configuration used in this study with acceptable accuracy from LES data. Turbulent fluctuations are held responsible, as they can generate spurious signal contributions at the monitor planes inside the computational domain, and also acoustic waves as they impinge on the outlet boundary of the domain.

Fortunately, it should be possible to eliminate the spurious contributions to the signals with the "Multi-Microphone Method" developed for the experimental determination of transfer matrices; see Paschereit & Polifke (1998). Acoustic waves generated at the outlet by turbulent fluctuations could actually be tolerated in transfer matrix estimation, unless they completely overwhelm in amplitude the upstream forcing signal. If this is the case, a thin "sponge layer" near the outlet could be used to dampen the amplitude of turbulent fluctuations impinging on the boundary (Lele (2002)). These modifications to the tranfer matrix estimation scheme and the boundary conditions shall be implemented in future work.

7. Acknowledgments

The Matlab-implementation of the Wiener-Hopf inverter used in this study was written by Alexander Genteman. Discussions with Summer Program participants and CTR staff, in particular Andre Kaufmann, Thierry Poinsot, Laurent Selle and Sanjiva Lele were exciting and enlightening. Thanks to Heinz Pitsch for reviewing this report. Financial support by the Center for Turbulence Research and the German Ministry for Education and Research (AG Turbo Project 4.4) is gratefully acknowledged.

REFERENCES

Bellanger, M. 1984 *Digital Processing of Signals*. Wiley Interscience.

Bohn, D. & Deuker, E. 1993 An acoustical model to predict combustion driven oscillations. In *20th Intl. Congr. on Combustion Engines*, **G20**. London, UK: CIMAC.

Deuker, E. 1995 Ein Beitrag zur Vorausberechnung des akustischen Stabilitätsverhaltens von Gasturbinen-Brennkammern mittels theoretischer und experimenteller Analyse von Brennkammerschwingungen. *PhD thesis*, RWTH Aachen.

Gentemann, A. M., Fischer, A. & Polifke, W. 2003 Acoustic transfer matrix reconstruction. In preparation.

Krüger, U., Hoffmann, S., Krebs, W., Judith, H., Bohn, D. & Matouschek, G. Stockholm, Sweden, 1998 Influence of turbulence on the dynamic behaviour of premixed flames. *ASME paper* 98-GT-323.

Lele, S. 2002 Private communication.

Ljung, L. 1999 *System Identification-Theory For the User*. Prentice Hall, 2nd Edition.

Paschereit, C. O. & Polifke, W. 1998 Investigation of the thermo-acoustic characteristics of a lean premixed gas turbine burner. In *Int'l Gas Turbine and Aeroengine Congress & Exposition*. Stockholm, Sweden.

Pierce, C. D. 2001 Progress-variable approach for large-eddy simulation of turbulent combustion. *PhD thesis*, Stanford University.

Poinsot, T. & Lele, S. K. 1992 Boundary conditions for direct simulation of compressible viscous flows. *J. Comp. Phys.* **101**, 104–129.

Poinsot, T. & Veynante, D. 2001 *Theoretical and Numerical Combustion*. R. T. Edwards, Inc.

Polifke, W., Paschereit, C. O. & Döbbeling, K. 2001*a* Constructive and destructive interference of acoustic and entropy waves in a premixed combustor with a choked exit. *Int. J. of Acoustics and Vibration* **6**, 135–146.

Polifke, W., Poncet, A., Paschereit, C. O. & Döbbeling, K. 1998 Determination of (thermo-)acoustic transfer matrices by time-dependent numerical simulation. *7th Int. Conference on Numerical Combustion*. York, UK.

Polifke, W., Poncet, A., Paschereit, C. O. & Döbbeling, K. 2001*b* Reconstruction of acoustic transfer matrices by instationary computational fluid dynamics. *J. Sound Vib.* **245**, 483–510.

Rabiner, L. R. & Gold, B. 1975 *Theory and Application of Digital Signal Processing*. Prentice Hall.

Selle, L. 2002 Private communication.

Thompson, K. W. 1987 Time dependent boundary conditions for hyperbolic systems. *J. Comp. Phys.* **68**, 1–24.

Wall, C., Pierce, C. D. & Moin, P. 2002 A semi-implicit method for resolution of acoustic waves in low mach number flows. *J. of Comp. Phys.* **181**, 545–563.